

Experimental Validation of a Bio-Inspired Controller for Dynamic Walking with a Humanoid Robot

Nicolas Van der Noot^{1,2}, Luca Colasanto², Allan Barrea³,
Jesse van den Kieboom², Renaud Ronsse¹ and Auke J. Ijspeert²

Abstract—Bipedal walking with humanoid robots requires efficient real-time control. Nowadays, most bipedal robots require to ensure local stability at every instant in time, preventing them from achieving the impressive human walking skills. At the same time, bio-inspired walking controllers are emerging, though they are still mostly explored in simulation studies. However, porting these controllers to real hardware is needed to validate their use on real robots, as well as adapting them to face the world non-idealities. Here, we implemented one of them on a real humanoid robot, namely the COMAN, by conducting dynamic walking experiments. More precisely, we used a muscle-reflex model producing efficient and human-like gaits. Starting from an off-line optimization performed in simulation, we present the controller implementation, focussing on the additional steps required to port it to real hardware. In our experimental results, we highlight some discrepancies between simulation and reality, together with possible controller extensions to fix them. Despite these differences, the real robot still managed to perform dynamic walking. On top of that, its gait exhibited stretched legs and foot roll at some points of the gait, two human walking features hard to achieve with most robot gaits. We present this on a 50 steps walk where the robot was free to move in the sagittal plane while lateral balance was provided by a human operator.

I. INTRODUCTION

While opportunities for using mobile robots are steadily expanding, the necessity to adapt the environment to these robots slows down their integration in our everyday life. In a world designed for humans, using humanoid robots could be a solution, since they can cope with our natural environment [1]. However, they are still far from reaching the impressive human performances, e.g. regarding walking. This prevents them from being extensively used in our day-to-day life.

Different methods can be used to achieve dynamic walking with a robot. Likely, the most famous ones are based on the zero-moment point (ZMP) which can be used as an indicator of gait feasibility [2]. Many experimental validations were conducted to make humanoid robots walk with ZMP-based methods, for example with ASIMO [3] or the HRP-2 platform [4].

This work was supported by the Belgian F.R.S.-FNRS (Aspirant #16744574 awarded to NVdN, Crédit aux Chercheurs #6809010 awarded to RR) and by the European Community's Seventh Framework Programme under Grant 611832 (WALK-MAN) and Grant 611626 (SYMBITRON).

¹Center for Research in Energy and Mechatronics, Institute of Mechanics, Materials and Civil Engineering, Université catholique de Louvain, B-1348 Louvain-la-Neuve, Belgium.

²Biorobotics Laboratory, Institute of Bioengineering, École Polytechnique Fédérale de Lausanne, CH-1015 Lausanne, Switzerland.

³Institute of Neuroscience and Institute of Information and Communication Technologies, Electronics and Applied Mathematics, Université catholique de Louvain, B-1348 Louvain-la-Neuve, Belgium.

However, there are important drawbacks associated with these control methods like energy inefficiency [5]. Moreover, these robots usually exhibit non human-like features like low waist position, constant knee flexion and foot surface kept parallel to the ground [6]-[7]. Even if some mechanical factors may explain these discrepancies, the main reasons are related to control strategies like singularity avoidance [6]. In particular, ZMP-based controllers require full local controllability (i.e. local stability is ensured at every instant in time), which is not necessary for stable walking, therefore consuming more energy [5].

The alternative concept called *limit cycle walking* adopts the perspective of relaxing constraints by considering the gait as a limit cycle and focussing on its global stability [8]. Bio-inspired controllers are emerging as a promising way to implement limit cycle walking. For instance, Shimoda et al. achieved robust reflex-based gaits on a humanoid robot for slow speeds (less than 1 cm/s) [9]. Another bio-inspired approach, developed by Geyer and Herr [10], presents a simplified model of human locomotion being exclusively controlled by a chain of reflexes and muscles encoding principles of legged dynamics. This approach converges to a muscle-reflex model producing efficient and realistic walking gaits for the normal human range of speed. Moreover, the simulated viscoelastic properties of these muscles provide robustness to environment perturbations. It was for instance adapted to be the central layer of the control architecture of a powered ankle-foot prosthesis [11].

In this paper, we adopt and extend the approach of [10]. This bio-inspired reflex-based controller has already been thoroughly studied in simulation [12]-[13]. In contrast, no study reports its implementation on a real full-body robot for human-like speed, to the best of our knowledge. The contributions of this paper are (i) the implementation of this reflex-based bio-inspired controller to a real humanoid robot, namely the COMAN, focussing on the additional steps required to port it to real hardware; (ii) the achievement of a human-like robot walking gait in the sagittal plane, to highlight the benefits of such a controller for bipedal walking; and (iii) a study of the discrepancies between simulation and reality, along with some clues to fix them.

Implementing this kind of controller on a real robot is not straightforward and new challenges appear with respect to scenarios limited to simulation environments: (i) working on real hardware requires to cope with the non-idealities of the real environment, such as highly non-linear joint friction torques or inaccurate torque tracking; (ii) reflex rules from

[10] only address the problem of 2D walking gaits, which is straightforward to get in simulation, but not on real hardware; and (iii) the experimental procedure is more likely to damage the robot and more difficult to automate. Our strategy is first to develop and optimize the controller in simulation under realistic assumptions, with the purpose to minimize the reality gap. Then, this controller is transferred to the real robot, without any additional tuning.

This paper is organized as follows. In section II, we introduce the COMAN, the robot used for dynamic walking, and the simulation environment. In section III, we provide an overview of the controller, focussing on its implementation on real hardware. In section IV, we show the results on a 50 steps walk performed by the robot, assessing its qualitative global behaviour and comparing it to the simulation results. Finally, section V concludes the paper.

II. HARDWARE AND SOFTWARE

An accurate simulation model of the COMAN is needed to develop the controller. We overview the robot hardware before presenting its simulation environment modelling.

A. COMAN platform

The COMpliant huMANoid (COMAN) is a 23 degrees of freedom (DOFs) full-body humanoid robot. This 95 cm tall robot, weighting 31 kg, was developed by the Italian Institute of Technology (IIT) [14]-[15]. COMAN is pictured in Fig. 1, along with the inertial base, relative joint frames and the world planes used to describe its kinematics.

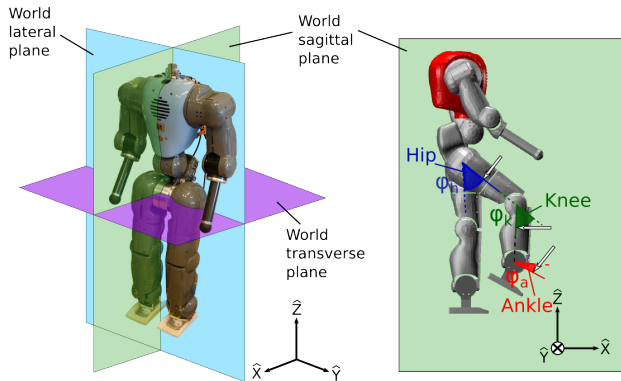


Fig. 1: Real COMAN along with the world planes and an inertial frame (left panel). Simulated COMAN in the world sagittal plane with an inertial frame and the leg sagittal joints (right panel). On the right side, the arrows indicate the direction of increasing angles. In this case, the hip angle is negative while both other angles are positive.

The three sagittal joints in each leg (see Fig. 1) feature series elastic actuators (SEA) [16], while the three remaining leg joints are actuated using traditional, stiff actuators.

Regarding the robot sensors, each joint features position encoders, along with custom-made torque sensors. The torque tracking is then achieved with a PI controller [17]. On top of that, custom-made 6 axis force/torque sensors are placed below the ankle joint to capture the ground interaction forces and torques. Finally, an inertial measurement unit (IMU) is attached to the robot waist.

B. Simulation environment

Section I identified several challenges related to the direct development of a bio-inspired controller on real hardware. Consequently, its development and optimization were first performed using a simulator modelling the COMAN in its environment. Next, the same controller can be transferred to the real robot.

The simulation suite, called Robotran [18], is an environment for multi-body systems developed within the Université catholique de Louvain. Its direct dynamics module is used to generate the symbolic equations of the robot dynamics. COMAN in Robotran is displayed in the right panel of Fig. 1. To further minimize the gap between simulation and reality, we reserved particular attention to the ground contact model (GCM), the actuator dynamics and the signals noise.

Regarding GCM, we adopt nonlinear spring-damper models with realistic friction forces, as described in [14]. An accurate and realistic GCM is critical because the resulting forces are important inputs of the controller (see section III-B). In this contribution, we do not cover the problem of lateral dynamic stability, focussing on the so-called 2D walking gait. In simulation, we constrain the waist to stay in the world sagittal plane (see Fig. 1).

In contrast to the simplified seven-segments model used in [10], our simulation purpose is to develop a controller able to run on the real robot. This involves dealing with motor and sensor noise. The series elastic actuator dynamics significantly affects the robot dynamics and should therefore be carefully modelled. Their implementation in simulation is fully described in [14]. Receiving a control voltage signal, each motor generates a torque at the joint level in a similar way for both the real and the simulated COMAN.

Regarding sensors information, we only use inputs available on the real robot (see section II-A). Preliminary experiments revealed that the torque is the signal being the most affected by noise. Consequently, a white noise with a maximal amplitude of 0.4 Nm was added to the torque reading in simulation. This corresponds to the noise being observed with the actual robot.

III. CONTROLLER IMPLEMENTATION

There are two main independent tasks in the controller: the lower-body and the upper-body ones, each of them sending position or torque references to a low-level controller. We briefly introduce this low-level controller before focussing on the lower-body and upper-body tasks. Then, we present the whole controller optimization.

A. Joints control

The joints controller is designed to track torque references or zero-position references (see sections III-B and III-C). This tracking is implemented on the real robot using a low-level controller described in [17]. The same low-level controller was replicated in simulation. Getting the appropriate voltage then reduces to compute appropriate position or torque references. The noise added in simulation on the torques reading directly impacts this part of the controller.

B. Lower-body control

Each leg is equipped with three sagittal joints (i.e. whose revolute axes are perpendicular to the sagittal plane) depicted in Fig. 1 and three non-sagittal joints (two lateral and one transverse). Control of all leg non-sagittal joints consists in tracking zero-position references, so that they can barely move during walking. Indeed, these joints are useful to maintain lateral dynamic stability, a problem which is not directly addressed in this contribution.

The leg sagittal joints propel the body forward during the walking gait. These joints are mainly controlled by the biological approach described in [10] and outlined here below. Seven muscle groups are identified within each leg (see Fig. 2, right panel). Because the COMAN does not have any muscle, we consider here virtual muscles whose state is computed as a set of equations.

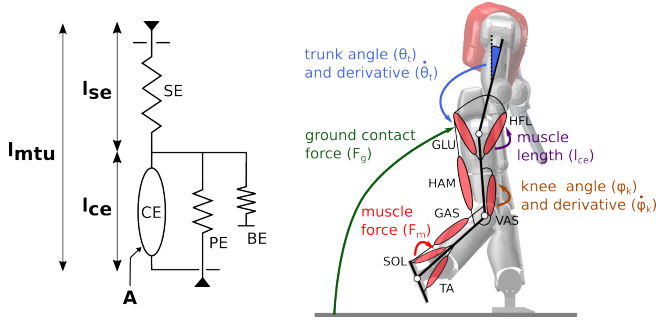


Fig. 2: Hill-type muscle (left panel). COMAN with the seven muscle groups of the right leg and some examples of reflex rules inputs (right panel). Some of these inputs only affect the stance leg. Muscles: soleus (SOL), tibialis anterior (TA), gastrocnemius (GAS), vasti (VAS), biarticular hamstring (HAM), gluteus (GLU) and hip flexor (HFL).

More precisely, we use the Hill-type model [19], presented in the left panel of Fig. 2. Each muscle tendon unit (MTU) consists of two main elements: a contractile one (CE) and a series elastic one (SE). On top of that, a parallel-elastic element (PE) and a buffer elasticity element (BE) only affect the muscle state outside its normal range of operation. Each virtual MTU attachment point to the real COMAN body is known, such that its length l_{mtu} can be directly computed from the sagittal joint angles φ (see Fig. 1). The length l_{ce} of CE depends on an extra input: the muscle activation A , which is detailed later. The length l_{se} of SE is computed as $l_{se} = l_{mtu} - l_{ce}$ and is directly related to the force F_m produced by the muscle. Finally, this force F_m generates a torque contribution τ_m on one or two joints (for the bi-articular muscles HAM and GAS) as $\tau_m = r_m(\varphi)F_m$, where $r_m(\varphi)$ is the lever arm. Full muscles implementation details can be found in [10] and [20]. To scale the muscles parameters to the size of the COMAN, we used dynamic scaling [21].

For each joint, the sum of all muscle torque contributions τ_m is sent as torque reference to the corresponding low-level controller presented in section III-A. The actual robot internal controller has a sampling period limited to 1 millisecond, which is too slow to cope with the muscle state integration, being governed by a stiff and strongly non-linear state equation [22]. Consequently, we integrate the

muscle model four times during each controller time step. Interestingly, this controller computation remains very fast (see section IV-D), despite these additional iterations.

The muscle activations A are related to neural inputs S called muscle stimulations, using a first-order low-pass filter capturing the excitation-contraction coupling, presented in (1) where τ is a time constant.

$$\tau \frac{dA}{dt} = S - A \quad (1)$$

Some examples highlighting how key stimulation contributions S_i are computed are described in (2), (3) and (4), focussing on their relations with the robot inputs. They are also visible in the right panel of Fig. 2. Summing these contributions S_i on each muscle produces their corresponding stimulation S . All parameters with index *opt* are parameters to be optimized (see section III-D). The whole description of stimulation computation is provided in [10].

$$S_i = k_{F,opt} F_m \quad ; \quad S_i = k_{l,opt} (l_{ce} - l_{opt}) \quad (2)$$

$$S_i = k_{g,opt} F_g (k_{\theta,opt} (\theta_t - \theta_{opt}) + k_{\dot{\theta},opt} \dot{\theta}_t) \quad (3)$$

$$S_i = k_{\varphi,opt} (\varphi_k - \varphi_{k,opt}) [\varphi_k < \varphi_{k,opt}] [\dot{\varphi}_k < 0] \quad (4)$$

The stimulations (2) capture reflex rules simply governed by the muscle states F_m and l_{ce} . The contribution of (3) stabilizes the trunk like an inverted pendulum, using the trunk angle θ_t and its derivative $\dot{\theta}_t$. On the COMAN, computing these two inputs requires to integrate signals provided by the IMU attached to the waist, while adding the trunk angles contribution using forward kinematics. The ground reaction forces F_g are available through the force sensors placed below the ankle joints. They are also used to trigger swing and stance phases. Finally, (4) inhibits the VAS muscles to prevent knee hyperextension. Its inputs are the knee angle φ_k and derivative $\dot{\varphi}_k$. Its activation is triggered only when the conditions displayed in the brackets are satisfied.

Preliminary tests revealed the prominent impact of non-linear joint friction torques in the real robot. Therefore, the computed muscle stimulations were typically too low to counteract these frictions (especially for the knee and ankle joints during swing motion). Modelling the joint friction is quite challenging and is not addressed in this contribution. However, we present one clue fixing the ankle joint issue.

Friction reduces ankle flexion during swing, hence deteriorating foot clearance with respect to the ground. This can result in an early touch of the foot on the ground. Consequently, the reflex rules from [10] were extended with an extra stimulation S_{TA}^+ feeding the TA muscle (see Fig. 2) during the swing phase: $S_{TA}^+ = k_{\varphi,a} (\varphi_a - \varphi_{a,th})$ where φ_a is the ankle position (see Fig. 1) while $k_{\varphi,a}$ (set to 4) and $\varphi_{a,th}$ (set to -0.1 rad) are two parameters manually tuned. This extra stimulation was added after the optimization process in order to prevent their minimization since they impose an unnecessary cost to the frictionless joint model. This affected the simulation gait, reducing its speed.

The reflex rules governing the knee dynamics were kept similar to those of [10], despite unmodelled friction. The impact of this will be discussed in section IV-C.

C. Upper-body control

The upper-body is made of eleven joints: four joints for each arm (shoulder roll, pitch, yaw and elbow) and three joints for the trunk. In general, the upper-body control is used to provide lateral balance to the walker. In simulation, this is not needed because of the 2D walking constraint (see section II-B). Consequently, we track constant position references for all these joints. Hence, the pose of the arms does not change.

On the real robot, another strategy was implemented to provide lateral balance, involving the upper-limbs. The main purpose is to let a human operator grab the wrists of the robot to provide lateral balance with a limited effect (ideally null) on the sagittal plane motion. This behaviour is achieved using Cartesian space impedance controllers on both arms of the robot [23] to keep them loosely only in the sagittal plane and stiff in the lateral direction. At the same time, the trunk joints are fixed using zero-position tracking. The same controller is implemented for each arm. The yaw shoulder joint is fixed to a constant position and the control torques of the remaining three joints can be expressed as follows:

$$\tau_{arm} = J^T(q_{arm})K_C(x_{des} - x) - D_J\dot{q}_{arm} \quad (5)$$

where $q_{arm}, \dot{q}_{arm}, \tau_{arm} \in \mathbb{R}^3$ are respectively the joint position, velocity and torque vectors and $x_{des}, x \in \mathbb{R}^3$ are respectively the Cartesian desired and actual positions of the wrist (with respect to a base reference frame with the origin at the pelvis of the robot and oriented as the inertial base in Fig. 1). $J(q_{arm}) \in \mathbb{R}^{3 \times 3}$ is the Jacobian of the wrist position in the same base frame and $K_C = \text{diag}(k_x, k_y, k_z) \in \mathbb{R}^{3 \times 3}$ is the Cartesian stiffness matrix. It collects the desired stiffness along the x, y and z directions of the base frame. $D_J = \text{diag}(d_{q_1}, d_{q_2}, d_{q_3}) \in \mathbb{R}^{3 \times 3}$ is the joint damping matrix collecting the damping for the three joints of the arm. The stiffness matrix and the damping matrix are positive-definite.

The first term of (5) maps into the arm joint space a force being proportional to the wrist position error according to the selected stiffness. The second term adds damping directly at the joint level to limit the joint velocities and stabilize the whole system. The desired behaviour is achieved using high stiffness values along the lateral direction ($k_y = 500 \text{ N/m}$) and zero stiffness along the sagittal directions ($k_x = k_z = 0 \text{ N/m}$). Finally, a low value is used for the damping of all the joints ($d_* = 0.1 \text{ (Nm s)/rad}$). In this way, the robot wrists can freely move in planes parallel to the sagittal one.

This impedance-based strategy turned to be a more viable solution for a treadmill-based experimental setup in regards to other existing solutions, like e.g. using a boom constraining the robot on a circular path [24].

D. Controller optimization

The lower-body controller design includes many open parameters (see section III-B and [10]), which must be properly tuned in order to first generate a stable walking gait, and then to optimize the gait efficiency. This tuning is performed in simulation with an extensive off-line optimization process using a heuristic optimization algorithm called *particle swarm optimization* (PSO) [25]. The optimization

process simulates a maximum 60 s walking gait. Sufficient foot clearance with the ground is guaranteed by adding bumps in the simulation environment during the optimization process. These bumps are trapezoidal shapes placed under the swing foot, next to the stance one. Their height linearly increases from 0 cm to 2 cm. This ensures that the swing foot lower extremity is at least 2 cm above the ground when both feet are next to each other (the most critical moment for ground clearance).

Each set of parameters is tested according to a staged objective function, i.e. different objectives are sorted by order of relevance so that the next objective is taken into account only when the previous one is fulfilled. At first, the robot must walk without falling, the objective function being proportional to the walking time. When it is able to walk during the 60 s simulation run, the forward speed is driven towards an arbitrary target speed of 0.5 m/s, which is a reasonable speed according to the robot height. The objective function f is computed as follows:

$$f = \alpha e^{-\beta(x-x_{des})^2} \quad (6)$$

where x is the forward speed, x_{des} the target speed and α, β two weight parameters. This function provides a result bounded between 0 and α . When the robot speed lies within a range of 0.05 m/s around the target speed, we minimize the metabolic energy consumption in the virtual muscles contraction per unit distance walked [26], again using (6). However, x now represents the metabolic energy consumption per unit distance walked while x_{des} is equal to zero, in order to minimize the absolute energy expenditure.

The noise added in the simulation environment (see section II-B) makes the optimizer converge to robust controllers. This is essential for experiments with real robots.

IV. RESULTS

We transferred the controller presented in section III directly to the real COMAN, without any additional tuning of the optimized parameters. Running it on real hardware led to a successful walking experiment. We present this on a 50 steps walk in the multimedia attachment. We first present the experimental setup and assess the lateral balance controller before comparing the experimental gait with the simulation results. Finally, we detail some specific features of this gait controller implemented on the real hardware.

A. Experimental setup

The main challenge of the experiments conducted with the real robot was to maintain its waist in the world sagittal plane, in order to reproduce the 2D walking gait generated in simulation. The adopted solution consists in using the impedance controller described in section III-C so that a human operator provides the lateral balance with a limited effect on the sagittal motion. The operator grabs the wrists which can freely move in planes parallel to the sagittal one (see Fig. 3 and the multimedia attachment).

The robot was initially suspended above a treadmill, from a hook located in the robot neck and connected to a pulley.

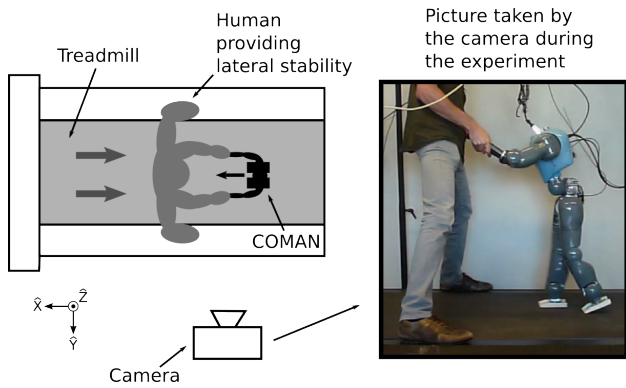


Fig. 3: Experimental setup for testing the COMAN dynamic walking. The robot was walking on a treadmill while a human operator placed in front of it provided lateral stability. A camera was used to capture the sagittal plane motion presented in the multimedia attachment.

Then, the robot was moved down such that an initial contact between the robot feet and the running treadmill initiated the reflex chain, and so the walking gait. In steady-state, the suspension rope did not interfere with the robot motion. The whole experimental setup is illustrated in Fig. 3.

In simulation, the robot speed was around 0.4 m/s, due to the extra TA stimulation added after the optimization (see section III-B). To match the real robot speed, the treadmill speed was set to 0.2 m/s, so two times smaller than the one obtained in simulation. This requirement for a lower experimental speed is explained in section IV-C.

B. Lateral balance

In the multimedia attachment, a first trial resulted in a fall of the robot in the sagittal plane after a few steps, due to a contact between the swing leg and the ground. This indicates that the lateral support provided by the operator is only ensuring stability in the lateral plane (as expected) and that the robot is alone in charge of its stability in the sagittal plane.

The effects of the lateral balance support on the sagittal plane can further be quantified by reporting the forces generated by the upper-body impedance controller on the arms during walking. Fig. 4 shows these forces for the left arm. Opposite forces with the same magnitude are generated at the waist of the robot, which is coherent with the action-reaction chain. The lateral force \hat{Y} (in blue) is two orders of magnitude larger than the frontal \hat{X} and vertical \hat{Z} forces (respectively in green and red). In fact, due to the stiffness values reported in section III-C, the movement of the hands, operated by the human, induced significant forces along the \hat{Y} direction only (see Fig. 3). The forces along the \hat{X} and \hat{Z} axes were only generated by the joints damping. This result thus validates the fact that the human assistance barely impacted the robot motion in the sagittal plane and so that lateral support did not affect the 2D walking. The robot was thus free to move and to fall in the sagittal plane, as it actually happened from time to time (see multimedia attachment).

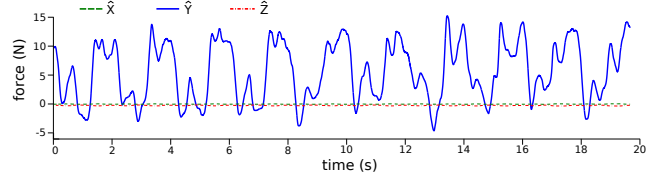


Fig. 4: The force amplitude along the lateral \hat{Y} direction is much bigger than the forces along the frontal \hat{X} and vertical \hat{Z} directions (measured on the left arm during ten strides).

C. Comparison between simulation and experimental results

Fig. 5 shows nine snapshots of the simulated COMAN with the selected optimal settings and the extra ankle stimulations presented in section III-B. These snapshots span a time frame of 1.46 s, corresponding to one stride starting at left foot strike. The same controller transferred to the real COMAN led to the gait shown in the snapshots of Fig. 6. These snapshots also present one stride starting at left foot strike, although spanning a longer time frame of 2.03 s. Both the simulated and real walking gaits are visible in the multimedia attachment.

The major difference between the simulated and the real gaits is the forward speed: 0.4 m/s in simulation against 0.2 m/s on the real robot (treadmill speed). Indeed, the real COMAN exhibits shorter steps with a lower frequency, as can be observed when comparing Figs. 5 and 6. The behaviour of the stance and swing legs during swing initiation is qualitatively similar in these two figures. However, this is not the case for the swing leg in late swing phase (compare snapshots (d) and (h) in these two figures). Indeed, while the knee is stretched in simulation, this is not the case with the real COMAN. This is likely due to the joint friction torques that were not modelled in the simulation environment. Consequently, the leg is never fully stretched during the swing phase, resulting in smaller steps. On top of that, a flexed swing leg is shorter than a stretched one. Consequently, impact with the ground happens later and induces a lower gait frequency on the real robot. So, these shorter steps combined with their slower frequency decrease the robot forward speed from 0.4 m/s to 0.2 m/s. The joint friction torques (and possibly other effects like no perfect motor back-EMF compensation) have thus a large impact on the resulting gait, also preventing heel strikes to appear. However, despite this difference in forward speed, the real robot was able to perform 50 steps, without any additional controller tuning. This demonstrates an impressive level of robustness of this bio-inspired controller, despite the external perturbations and unmodelled dynamics.

Fig. 7 and Fig. 8 show the actual positions, torques, and ground reaction forces captured during two strides of these walking trials, for both the simulated and the real COMAN. These graphs follow the conventions depicted in the right panel of Fig. 1. Despite the significant difference in the cycle duration, the gait kinematics is quite similar between the simulated and the real COMAN (compare panels (a) and (b) in Fig. 7). In particular, the hip trajectories are barely distinguishable. In both cases, the knee trajectory

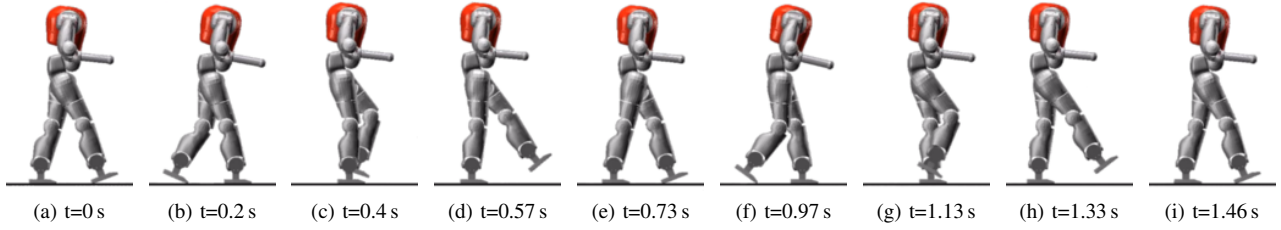


Fig. 5: Snapshots of the COMAN in the Robotran simulation environment, corresponding to panels (a) and (c) in Fig. 7 and (a) in Fig. 8. Snapshots (a), (e) and (i) are taken at foot strike, (b) and (f) at foot push-off, (c) and (g) when feet are adjacent and (d) and (h) during late swing.

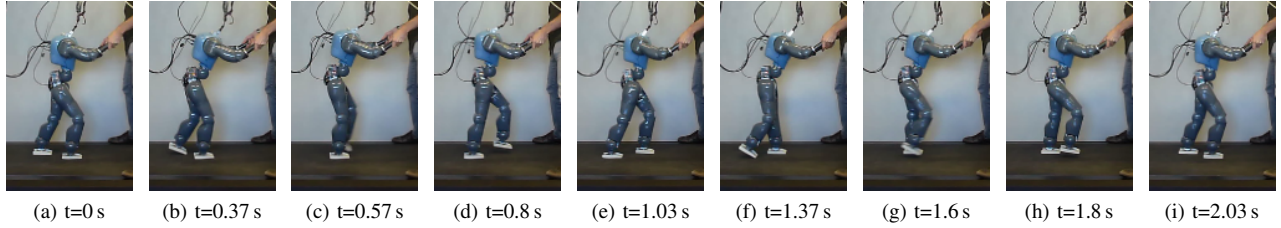


Fig. 6: Snapshots of the real COMAN, corresponding to Fig. 4, to panels (b) and (d) in Fig. 7, to panel (b) in Fig. 8 and to Fig. 9. These snapshots are consistent with the ones detailed in Fig. 5 (e.g. panel (a) is also taken at foot strike).

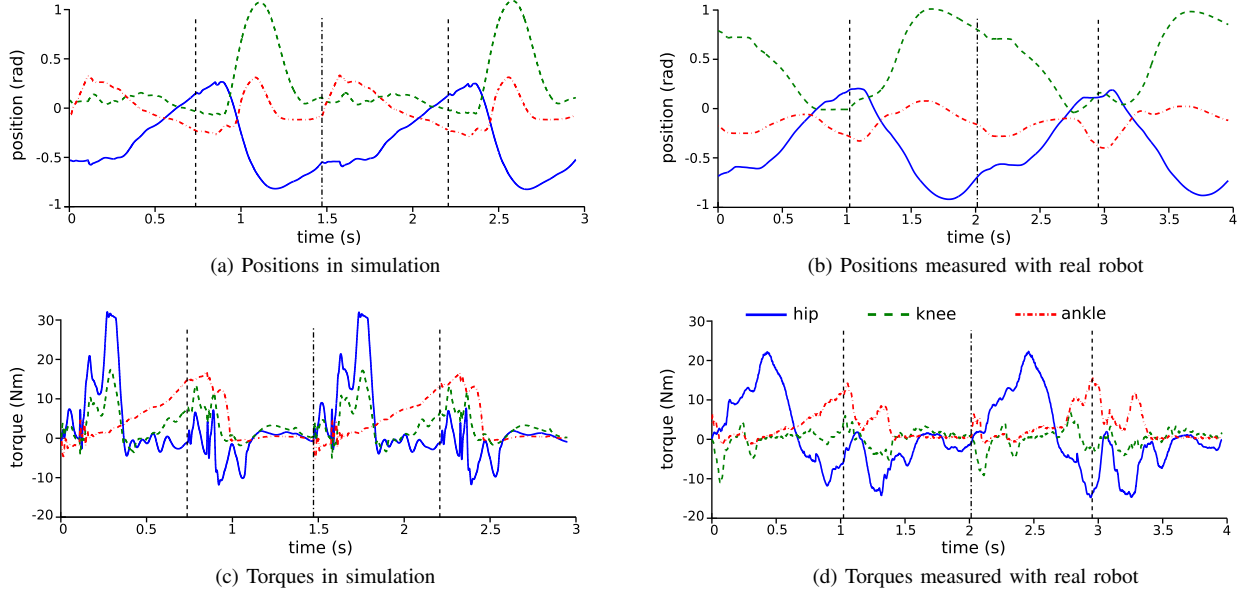


Fig. 7: Positions and torques on the COMAN for the left leg sagittal joints, both in simulation (left) and on the real robot (right), according to the conventions depicted in Fig. 1. The joint frames are depicted in Fig. 1. These graphs start at a left leg foot strike and span over two strides. Right strikes are indicated with dashed lines while the second left strike is indicated with a dashed line integrating dots. The time references are consistent with the ones presented in Fig. 5 (simulated robot) and Fig. 6 (real robot).

peaks during swing initiation but lasts longer on the real robot for the reasons phrased above. During a fraction of the stance phase, the knee position lies near zero for the real COMAN, indicating that the leg is stretched. This feature is usually not encountered in most humanoid robots to avoid controller singularities. Regarding the ankle, the pattern is more different. Indeed, this joint is more affected by the ground interactions. In contrast to many traditional ZMP-based walker, the robot feet are not always kept parallel to the ground. This is especially visible during swing initiation in snapshots (b) and (f) of Fig. 6. On top of that, it is interesting

to note that if the leg was stretched during the swing phase, the COMAN would hit the ground with the heel at foot strike, like humans do. Regarding torques, a proximodistal gradient also appears when analyzing simulation and reality matching: the hip matching is slightly better than the ankle one.

The global pattern of the ground reaction forces is again similar (see Fig. 8), except at foot strike where sharp variations happen in simulation, but not on real hardware. The reason is that the simulated ground contact model involves high and noisy peaks at foot strike, due to the stiff spring-damper contact model used [14].

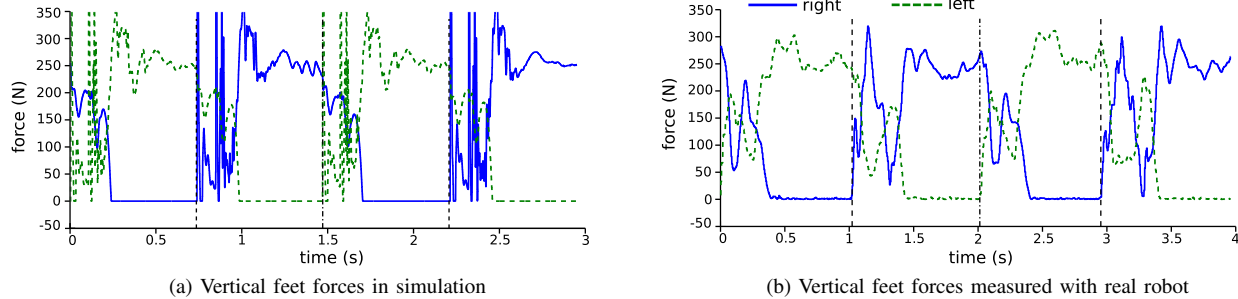


Fig. 8: Vertical foot forces, both in simulation (left) and on the real robot (right). The time references are consistent with the ones in Fig. 7.

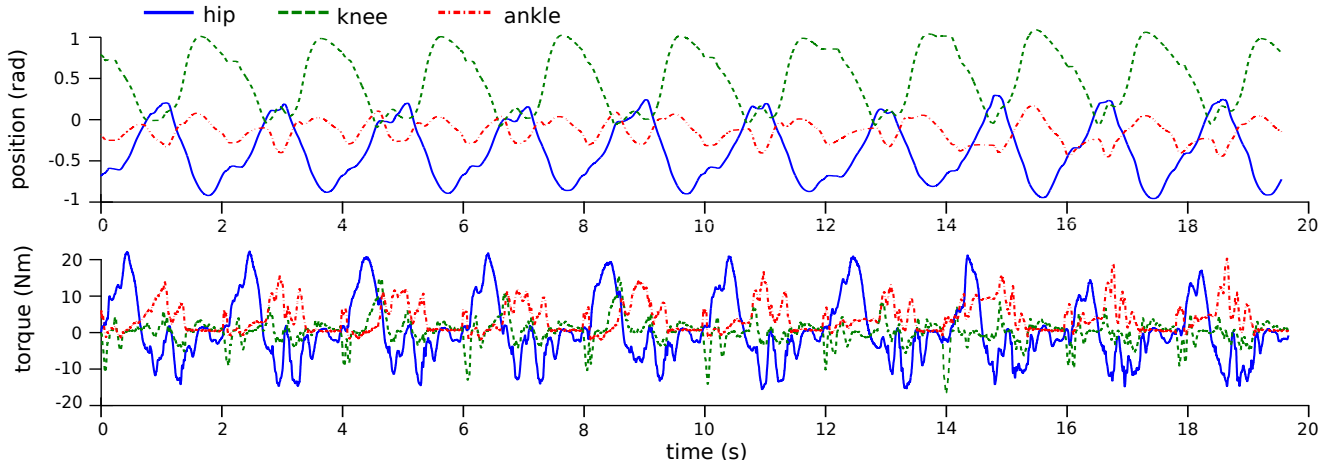


Fig. 9: Positions and torques on the real COMAN left leg sagittal joints, according to the conventions depicted in Fig. 1. These graphs start at a left leg foot strike and span over ten strides. The time references are consistent with the one in Fig. 6.

D. Bio-inspired controller features

Some of the specific gait features emerging from this reflex-based bio-inspired controller were already identified in section IV-C, like foot roll and stretched knees during stance phase. Additionally, conventional ZMP-based walkers tend to walk conservatively by lowering the waist height [6]. This is not the case with our controller (see Fig. 6), due to the stretched stance leg. These human-like features also enable more energy-efficient walkers by taking more advantage from the inertia effects, but this remains to be quantified. Finally, the real COMAN gait showed a remarkable reproducibility over successive strides. This can be observed in Fig. 9 where positions and torques are displayed over ten strides.

Classical controllers, relying on inverse dynamics computation, require heavy computational process [5]. Consequently, fulfilling real time constraints is challenging. In this experiment, running one iteration of the whole lower-body bio-inspired controller was performed on average in $14.8 \mu s$. This was tested on a computer with dual-core Intel(R) Core(TM) i7-4600U CPU, 2.1GHz and 8 Go RAM. This is more than 67 times faster than the controller sampling rate, namely $1 ms$, which is another key advantage of this bio-inspired approach.

V. CONCLUSION

In this contribution, we presented an experimental gait on a humanoid robot walking with a bio-inspired controller, based on reflex rules. While this controller was already extensively studied in simulations, we brought it to a real full-body humanoid robot: the COMAN. We presented some extra steps to port it on real hardware, like actuator dynamics modelling, robustness to noise or real-time issues. Running experiments on the real robot highlighted the non-idealities of the real world, stressing the necessity to drive the controller design according to them. The major non-idealities were related to joint friction, especially at the knee and ankle levels. We focused on the impacts of friction on the gait pattern and we presented some clues to fix them.

Regarding the walking gait, we pointed out interesting controller features and compared them to classical approaches: fast computational rate, and similarities to key human gait features (stretched leg during stance phase, foot roll and higher waist position), which could lead to more energy-efficient robots. Moreover, this controller demonstrated some robustness when transferred from a frictionless joint model simulator to real hardware, without any controller re-tuning (robustness to external perturbations demonstrated in [10] still needs to be tested on the real robot). This was illustrated

on a 50 steps trial where lateral stability was provided by a human operator.

The reported results call for further developments. A first improvement would be to reduce the gap between simulation and reality by implementing joint friction effects in the simulation environment. Nonetheless, friction modelling is not trivial and would not solve the knee flexion issue during swing phase, due to the lack of corresponding stimulation control. A precise timing is required to stretch the leg, which is difficult to get on a pure reflex-based controller. Therefore, we are also exploring the addition of new muscles control principles, like the introduction of a central pattern generator (CPG) to predict the current gait cycle phase [13]. A CPG is a neural circuit found in both invertebrate and vertebrate animals, capable of producing rhythmic patterns of neural activity, receiving only tonic inputs [27].

Finally, the controller implemented only 2D walking gaits. We presented a new method to test these gaits on real robots without deploying complex boom structures like in [24]. We assessed the effectiveness of this approach by reporting almost zero interaction forces between the human operator and the robot in the sagittal plane, and by showing that human interventions did not prevent the robot from falling in this sagittal plane. Future developments should however focus on full 3D control (like the simulations results from [12]), rather than developing new experimental setups for 2D walking.

While bipedal robots are currently far from the walking capabilities of real humans in terms of robustness and energy-efficiency, this contribution shows that it is possible to take advantage of motor control mechanisms identified in humans to reproduce them on robotic devices, and so to get bipedal robot behaviours closer to human ones.

REFERENCES

- [1] S. Schaal, "The New Robotics-towards human-centered machines." *HFSP journal*, vol. 1, no. 2, pp. 115–26, July 2007.
- [2] M. Vukobratović and B. Borovac, "Zero-Moment Point - Thirty five years of its life," *International Journal of Humanoid Robotics*, vol. 01, no. 01, pp. 157–173, Mar. 2004.
- [3] J. Chestnutt, M. Lau, G. Cheung, J. Kuffner, J. Hodgins, and T. Kanade, "Footstep Planning for the Honda ASIMO Humanoid," in *Proceedings of the 2005 IEEE International Conference on Robotics and Automation*. IEEE, 2005, pp. 629–634.
- [4] K. Kaneko, F. Kanehiro, S. Kajita, K. Yokoyama, K. Akachi, T. Kawasaki, S. Ota, and T. Isozumi, "Design of prototype humanoid robotics platform for HRP," in *IEEE/RSJ International Conference on Intelligent Robots and System*, vol. 3. IEEE, 2002, pp. 2431–2436.
- [5] H. Dallali, "Modelling and dynamic stabilization of a compliant humanoid robot, CoMan," Ph.D. dissertation, University of Manchester, 2011.
- [6] R. Kurazume, S. Tanaka, M. Yamashita, T. Hasegawa, and K. Yoneda, "Straight legged walking of a biped robot," in *2005 IEEE/RSJ International Conference on Intelligent Robots and Systems*. IEEE, 2005, pp. 337–343.
- [7] P. Sardain and G. Bessonnet, "Zero Moment Point Measurements From a Human Walker Wearing Robot Feet as Shoes," *IEEE Transactions on Systems, Man, and Cybernetics - Part A: Systems and Humans*, vol. 34, no. 5, pp. 638–648, Sept. 2004.
- [8] D. G. Hobbelen and M. Wisse, *Humanoid Robots: Human-like Machines*. Vienna, Austria: I-Tech Education and Publishing, 2007.
- [9] S. Shimoda, Y. Yoshihara, and H. Kimura, "Adaptability of Tacit Learning in Bipedal Locomotion," *IEEE Transactions on Autonomous Mental Development*, vol. 5, no. 2, pp. 152–161, June 2013.
- [10] H. Geyer and H. Herr, "A muscle-reflex model that encodes principles of legged mechanics produces human walking dynamics and muscle activities." *IEEE transactions on neural systems and rehabilitation engineering : a publication of the IEEE Engineering in Medicine and Biology Society*, vol. 18, no. 3, pp. 263–73, June 2010.
- [11] M. F. Eilenberg, H. Geyer, and H. Herr, "Control of a powered ankle-foot prosthesis based on a neuromuscular model." *IEEE transactions on neural systems and rehabilitation engineering : a publication of the IEEE Engineering in Medicine and Biology Society*, vol. 18, no. 2, pp. 164–173, Apr. 2010.
- [12] J. M. Wang, S. R. Hamner, S. L. Delp, and V. Koltun, "Optimizing locomotion controllers using biologically-based actuators and objectives," *ACM Trans. Graph*, p. 25, 2012.
- [13] N. Van der Noot, A. J. Ijspeert, and R. Ronsse, "Biped gait controller for large speed variations, combining reflexes and a central pattern generator in a neuromuscular model," in *2015 IEEE International Conference on Robotics and Automation (ICRA)*, May 2015, pp. 6267–6274.
- [14] H. Dallali, M. Mosadeghzad, G. A. Medrano-Cerda, N. Docquier, P. Kormushev, N. Tsagarakis, Z. Li, and D. Caldwell, "Development of a dynamic simulator for a compliant humanoid robot based on a symbolic multibody approach," in *2013 IEEE International Conference on Mechatronics (ICM)*. IEEE, Feb. 2013, pp. 598–603.
- [15] N. G. Tsagarakis, S. Morfey, G. M. Cerda, Z. Li, and D. G. Caldwell, "COMAN a Compliant Humanoid: Optimal Joint Stiffness Tuning for Modal Frequency control," in *IEEE International Conference on Robotics and Automation, . Proceedings. ICRA '13.*, 2013.
- [16] N. G. Tsagarakis, M. Laffranchi, B. Vanderborght, and D. G. Caldwell, "A compact soft actuator unit for small scale human friendly robots," in *IEEE International Conference on Robotics and Automation, ICRA '09.*, 2009, pp. 4356–4362.
- [17] M. Mosadeghzad, G. A. Medrano-Cerda, J. A. Saglia, N. G. Tsagarakis, and D. G. Caldwell, "Comparison of various active impedance control approaches, modeling, implementation, passivity, stability and trade-offs," in *2012 IEEE/ASME International Conference on Advanced Intelligent Mechatronics (AIM)*. IEEE, July 2012, pp. 342–348.
- [18] J.-C. Samin and P. Fiset, *Symbolic Modeling of Multibody Systems*. Springer, 2004.
- [19] A. V. Hill, "The Heat of Shortening and the Dynamic Constants of Muscle," *Proceedings of the Royal Society B: Biological Sciences*, vol. 126, no. 843, pp. 136–195, Oct. 1938.
- [20] H. Geyer, A. Seyfarth, and R. Blickhan, "Positive force feedback in bouncing gaits?" *Proceedings. Biological sciences / The Royal Society*, vol. 270, no. 1529, pp. 2173–83, Oct. 2003.
- [21] A. Schepelmann, M. D. Taylor, and H. Geyer, "Development of a Testbed for Robotic Neuromuscular Controllers," in *Robotics: Science and Systems*. MIT Press, 2012.
- [22] N. Van der Noot, F. Dzeladini, A. J. Ijspeert, and R. Ronsse, "Simplification of the Hill Muscle Model Computation for Real-Time Walking Controllers with Large Time Steps," in *Dynamic Walking Conference*, ETH Zurich, 2014.
- [23] N. Hogan, "Impedance Control: An Approach to Manipulation: Part I-Theory, Part II-Implementation, Part III-Applications," *Journ al of Dynamic Systems, Measurement, and Control*, vol. 107, pp. 1–24, 1985.
- [24] T. Geng, B. Porr, and F. Wörgötter, "Fast biped walking with a reflexive controller and real-time policy searching," in *Advances in Neural Information Processing Systems*, 2005, pp. 427–434.
- [25] J. Kennedy and R. Eberhart, "Particle swarm optimization," in *Proceedings of ICNN'95 - International Conference on Neural Networks*, vol. 4. IEEE, 1995, pp. 1942–1948.
- [26] L. J. Bhargava, M. G. Pandy, and F. C. Anderson, "A phenomenological model for estimating metabolic energy consumption in muscle contraction," *Journal of Biomechanics*, vol. 37, no. 1, pp. 81–88, Jan. 2004.
- [27] A. J. Ijspeert, "Central pattern generators for locomotion control in animals and robots: A review," *Neural Networks*, vol. 21, no. 4, pp. 642–653, 2008.